Title

Distance-dependent dielectric constant at the calcite/electrolyte interface: Implication for surface complexation modeling

Author

Zarzycki, Piotr

Publication Date

2023-09-01

DOI

10.1016/j.jcis.2023.04.169

Distance-dependent dielectric constant at the calcite/electrolyte interface: implication for surface complexation modeling

Piotr Zarzycki,[1*]

[1]*Energy Geosciences Division, Lawrence Berkeley National Laboratory, 1 Cyclotron Road, Berkeley, California, United States*

Abstract

Hypothesis: The electrical double layer formed at the mineral/electrolyte interface is often modeled using mean-field approaches based on a continuum description of the solvent whose dielectric constant is assumed to decrease monotonically with decreasing distance to the surface. In contrast, molecular simulations show that the solvent polarizability oscillates near the surface similar to the water density profile – as shown previously, for example, by Bonthuis et al. (D.J. Bonthuis, S. Gekle, R.R. Netz, Dielectric Profile of Interfacial Water and its Effect on Double-Layer Capacitance, Phys Rev Lett 107(16) (2011) 166102). We showed that molecular and mesoscale pictures agree by spatially averaging the dielectric constant obtained from molecular dynamics simulations over the distances relevant to the mean-field representation. In addition, the values of capacitances used to describe the electrical double layer in Surface Complexation Models (SCMs) of the mineral/electrolyte interface can be estimated using molecularly informed spatially averaged dielectric constants and positions of hydration layers.
Experiments: First, we used molecular dynamics simulations to model the calcite $10\bar{1}4$/electrolyte interface. Next, by using atomistic trajectories, we calculated the distance-dependent static dielectric constant and water density in the direction normal to the. Finally, we applied spatial compartmentalization consistent with the model of parallel-plate capacitors connected in series to estimate SCM capacitances.
Findings: Computationally expensive simulations are required to determine the dielectric constant profile of interfacial water near the mineral surface. On the other hand, water density profiles are readily assessable from much shorter simulation trajectories. Our simulations confirmed that dielectric and water density oscillations at the interface are correlated. Here, we parametrized linear regression models to estimate the dielectric constant directly from the local water density. This is a significant computational shortcut compared to slowly converging calculations relying on total dipole moment fluctuations. The amplitude of the interfacial dielectric constant oscillation can exceed the dielectric constant of the bulk water, suggesting an ice-like frozen state, but only if there are no electrolyte ions. The interfacial accumulation of electrolyte ions causes a decrease in the dielectric constant due to the reduction of water density and re-orientation of water dipoles in ion hydration shells. Finally, we show how to use the computed dielectric properties to estimate SCM's capacitances.

Keywords: interfacial dielectric constant, capacitance, electric double layer, ice-like water, molecular dynamics, calcite/electrolyte interface

1. Introduction

The distribution of mobile and bound charges at the charged solid surface/electrolyte solution interface is referred to as the electric double layer (EDL). EDL is typically modeled using macroscopic, mean-field theories that consider a solvent as a dielectric continuum and project physicochemical properties onto the direction normal to the surface. In the approaches based on the Poisson-Boltzmann equation, tt lateral interactions and ion-ion correlations are neglected, and a mean-field-type electric potential is used to describe the effect of the surface charge on ion spatial distributions. Here, we focus on the Triple Layer Model (TLM) of EDL, in which the interfacial region is conceptually divided into compact and diffuse parts [1-4]. The compact part (Stern layer) consists of layers of localized charges, which, from the electrostatic point of view, are equivalent to the plates of parallel plate capacitors connected in series. The diffuse part is adjacent to the compact part, and it extends toward the bulk solution. From the mathematical point of view, the spatial distribution of ions in TLM is governed by Laplace (Stern part) and Poisson-Boltzmann (diffuse part) differential equations, respectively [3, 4].

*Corresponding author. Tel.: +1-510-486-6272; fax: +1-510-486-6455.
E-mail address: ppzarzycki@lbl.gov

To describe the charge distribution at the mineral/electrolyte interfaces, one needs to account for the variable surface charge, which depends on environmental conditions such as salt concentration, pH, and temperature. Combinations of geometric models of charge distribution and interfacial chemistries are known as the Surface Complexation Models (SCMs) [2, 3]. Currently, SCMs are invaluable in interpreting many electrochemical and sorption measurements and indispensable in analyzing the retention of contaminants, radionuclides, and heavy metals by soils [2, 3, 5].

Unfortunately, applying SCMs to experimental data in an ambiguous fashion is often challenging. Many SCM descriptors are not yet accessible experimentally and therefore treated as the best-fit parameters [6-8]. Moreover, interdependencies between model parameters hamper finding a unique and transferable solution to the SCM equations. Indeed, non-consistent and non-transferable parameter values have been reported by various research groups even if the same experimental dataset was analyzed [2,3]. Among many SCM parameters, the capacitances of hypothetical parallel-plate EDL capacitors are the most difficult to estimate accurately.

In the theoretical framework of the parallel-plate capacitor model, capacitance links the potential difference between layers of accumulated charges $\Delta\psi$ to the charge accumulated at a given layer σ (i.e., $c = \sigma/\Delta\psi$). The capacitance (c) quantifies the ability of a capacitor to store charge, and it is related to the dielectric constant of medium between plates (ϵ) and plates separation (d):

$$c = \epsilon_0 \, \epsilon/d \tag{1}$$

where ϵ_0 is the vacuum permittivity.

The physical interpretation of capacitance severely restricts a range of acceptable values, mainly due to a narrow range of physically possible values of the dielectric constant of the intervening medium. It has been assumed that water near the surface is in a dielectric saturation state, similar to the water in the first hydration shell of a small or highly charged ion [9, 10]. The dielectric saturation implies that most of the water-water hydrogen bonds are broken, and tetrahedral ordering disappears [9, 11]. Although the dielectric constant of water in the hydration layers cannot be directly measured, a theoretical minimum value was calculated assuming a hypothetical state of perfect alignment of all interfacial water dipoles with the field lines at the metallic electrode. The limiting value was set as equal to the high-frequency dielectric constant of water (~5.9 at room temperature) [9]. Within continuum-solvent frameworks on which SCMs are based, the dielectric constant is expected to be between 6 and 20 for the inner part of the EDL. It is also assumed that the dielectric constant increases monotonically with an increasing distance from the surface until the bulk value is recovered [5, 10, 12].

Unfortunately, the distance-dependent dielectric constant of the interfacial solution is not yet directly measurable. It is also challenging to unambiguously extract it from recorded collective signals in dielectric, impedance, or vibrational spectroscopies [13-16] or from theoretical model fitting to surface and atomic force measurements [17, 18]. A few indirect measurements confirm theoretical expectations of a low dielectric constant of confined or interfacial water. However, raw data analyses are often biased by an implicit assumption that interfacial ε is lower than in the bulk phase [13, 17, 18].

Surprisingly, molecular simulations of the distance-dependent dielectric constant contradict theoretically expected dielectric saturation at the interface. Instead, most simulation studies have reported an increase in the dielectric constant of water near the hydrophobic and hydrophilic surfaces and an oscillatory rather than monotonic distance-dependence [19-21]. Here, we address the apparent contradiction between theoretical expectations and computer simulations by exploring the mean-field nature of EDL models. Specifically, we projected the molecular dynamics simulations of the water dielectric properties as a function of distance from the mineral surface onto a spatial resolution of TLM's parallel-plate capacitors.

We focused on the calcite/electrolyte interface as one of the most challenging reactive interfaces for SCM-type description and representative of sediments and sedimentary rocks. The interfacial chemistry of carbonates is also essential because they host half of the world's oil and gas reserves [22]. The interfacial chemistry governs dissolution, (co)precipitation, crystal morphology/habits evolution, and mechanisms of the carbonate diagenesis [23]. Therefore, to understand the time evolutions of permeability and porosity in carbonate rocks and how to extract oil/gas more efficiently, one needs to understand the reactivity of carbonate/electrolyte interfaces.

2. Theory and Computation

2.1. Electric double-layer model of calcite/electrolyte interface

Calcite surfaces become electrically charged when in contact with an electrolyte solution. The surface charge is compensated by counter- and co-ions accumulated on the solution side of the interface. The origin of the surface charge and the nature of the potential determining ions (PDI) for the calcite/electrolyte interface have been debated in the past [24, 25]. It is widely accepted that the calcite constitutive ions, carbonate, and calcium are the primary PDI [26-28]. The H^+ and OH^- ions are considered secondary PDI because they govern the speciation of carbonate and calcite at the surface and in bulk and thus indirectly affect the surface charge [26-29]. Many electrolyte ions also form strong complexes with calcium and carbonate ions (e.g., Cl^- [25], U^{4+}, UO_2^{2+}) and can be considered tertiary PDI.

To construct SCM, one needs to adopt a geometric model of the spatial charge distribution in addition to a model of interfacial chemistry. In the case of the calcite/electrolyte interface, models with only one parallel-plate capacitor (Basic Stern Model, BSM) [27, 28] or two capacitors connected in series (Triple Layer Model, TLM) [30] have been successfully applied to analyze experimental observations (see Fig. 1). The capacitances are defined as a ratio of the accumulated charge on one of the plates to the potential drop across the dielectric medium between the plates (Eq. 1). By using parallel plate capacitors, one reduces the number of unknowns and makes a set of SCM equations solvable. Specifically, instead of independently determining electrostatic potentials in each layer, only the diffuse layer potential (ψ_d) is calculated, and then it is backpropagated to β- and surface layers (ψ_β, ψ_0) through charge densities (σ_0, σ_d) and capacitances (c_1, c_2), that is:

$$\psi_0 = \psi_\beta + \frac{\sigma_0}{c_1} = \psi_d - \frac{\sigma_d}{c_2} + \frac{\sigma_0}{c_1} \quad (2)$$

The capacitance value of the dielectric phase between the surface and β-plane (c_1) is assumed to be low (e.g., 0.5 F/m^2). This assumption is based on the notion that water near the surface is in a dielectric saturation state. In this state, the electric field generated by the surface charge and accumulated ions restrict water mobility and reduce the dielectric constant to values between 6 and 10 [2, 3]. However, in the case of the calcite/electrolyte interface, much larger capacitance values have been reported. For example, Van Cappellen et al. [31] used capacitances equal to 30 F/m^2 and 168 F/m^2 for diluted and concentrated solutions, respectively. Pokrovsky and Schott [32] used a capacitance equal to 17 F/m^2 for $CaCO_3$, and an even larger value (31 F/m^2) for $MgCO_3$, $FeCO_3$, $CoCO_3$, and $NiCO_3$ surfaces. Unfortunately, these values correspond to the dielectric constant exceeding the acceptable bulk water range. As Heberling et. al. [26] pointed out, the unrealistically high value of capacitance is one of the major drawbacks of many early SCMs developed for carbonate mineral/electrolyte interfaces. A few more recent SCMs thrive to realistically reproduce the interfacial water dielectric state, keeping the capacitance value fixed around 0.45 F/m^2 (ε between 12 and 18) [27, 28, 33].

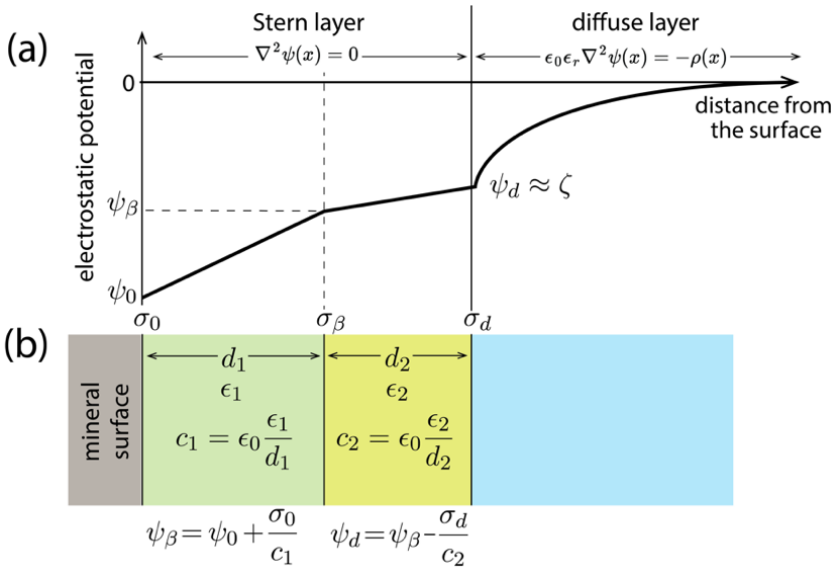

Figure 1. The schematic illustration of the electric double layer model of the mineral/electrolyte interface [27, 28, 33-35]. The magnitude of the electrostatic potential decreases with increasing distance from the surface in a linear fashion within the Stern layer according to the Laplace equation and in an exponential fashion in the diffuse layer according to the Poisson equation (a). The Stern part of the EDL is modeled as two parallel-plate capacitors, or molecular condensers, connected in series (b).

On the one hand, a few indirect experimental measurements agree with the notion of dielectric saturation at the interface [13-18]. On the other hand, molecular simulations claim that the dielectric constant of any polar fluid near fluid/solid interfaces can be much larger than in the bulk phase [19-21]. In other words, molecular simulations suggest partial freezing of the interfacial water rather than its dielectric saturation. A few experimental reports of ice-like water structure formation in the first hydration sheet at the mineral surfaces corroborate with molecular simulations [36-38].

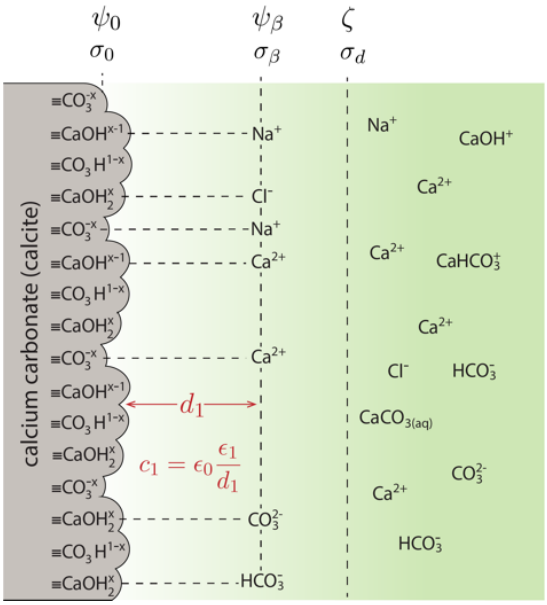

Figure 2. Scheme of the Basic Stern Surface Complexation Model of the calcite ($10\bar{1}4$)/NaCl electrolyte interface as developed by Heberling et al. [27, 28] – here used to illustrate the molecular-simulation-based parametrization of the values of EDL capacitances.

2.2. Surface Complexation Model of the calcite (**10$\bar{1}$4**)*/electrolyte interface*

Several SCMs have been developed for the calcite/electrolyte interface [27-29, 31, 39]. They differ in assumed charging mechanisms and stoichiometries of the surface groups/complexes. Here, we used the model developed by Heberling et al. [27, 28], which is based on a combination of the Charge Distribution Multisite Complexation model (CD-MUSIC) and the BSM description of the EDL. This model considers the pH-dependent ion-pair formation and carbonate speciation in the bulk phase, surface protonation, and deprotonation considering two primary surface site types $\equiv CO_3H^{1-x}$ and $\equiv CaOH^{x-1}$. The electrolyte ions (e.g., Na^+, Cl^-) and constituent ions (Ca^{2+}, CO_3^{2-}) are accumulated as the outer-sphere complexes in the b-plane (Fig. 2). One of the advantages of BSM is the presence of only one capacitance, c_1. The protonation and complexation reactions considered in this model are taken from Heberling et al. [27, 28], and they are listed in Table S1 in the Supporting Information. Here, we used SCM only to illustrate how differences in the inner layer capacitance and interfacial water dielectric constant translate to variation in the charge and potential distributions and ion speciation in the EDL.

2.3. Calcite (**10$\bar{1}$4**)*/aqueous solution interface*

Calcite is the most stable polymorphic form of calcium carbonate [40]. It crystallizes in a rhombohedral system and forms trigonal prismatic crystals with rhombohedral, prismatic, or scalenohedral terminations. The cleavage along the 10$\bar{1}$4 axis is the most common; therefore, the 10$\bar{1}$4 crystal face dominates the properties of the carbonate crystal particles. The 10$\bar{1}$4 surface consists of alternating rows of carbonate and calcium ions leading to the charge-neutral surface. To model the calcite (10$\bar{1}$4)/electrolyte interface, we prepared a thick calcite slab terminated on both sides by (10$\bar{1}$4) face and immersed it in the aqueous solution (Fig. 3).

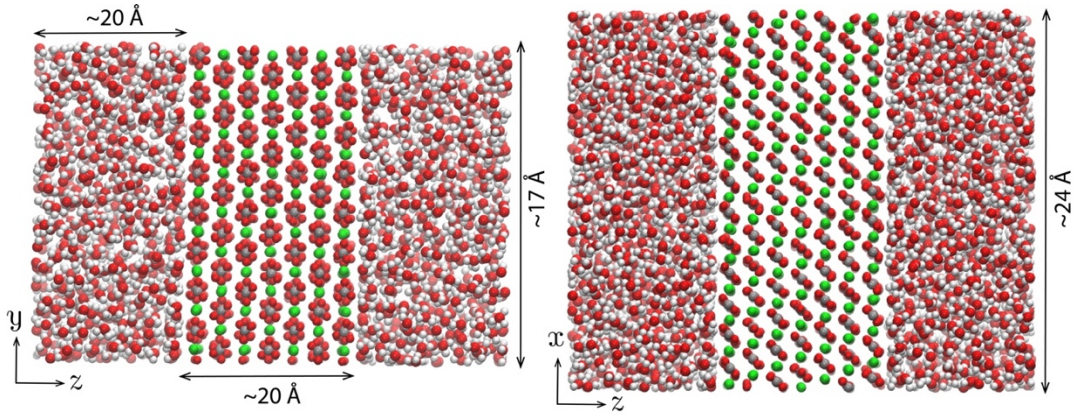

Figure 3. Molecular representation of the calcite (10$\bar{1}$4) crystal faces exposed to aqueous solution employed in the molecular dynamics simulation in this study (rotated snapshots).

2.4. Molecular Dynamics Simulation

Many molecular simulation studies of calcite and calcite/electrolyte interfaces have been reported in the last decade [41-64]. They differ in how the inter- and intramolecular interactions are described and the level of theory involved in the computation. This work used classical molecular dynamics simulations with a polarizable force field for the calcite/electrolyte solution developed by de Leeuw and Parker [43]. However, the water phase was modeled using the three-point rigid OPC3 water model [65] to improve the description of water dielectric properties [66]. The force-field parameters for Na^+ and Cl^- ions are taken from Sengupta et al. [67, 68]. The geometry of the calcite/solution interface was optimized using a gradient descent algorithm until the energy change was below 10^{-6} kcal/mol. Next, the simulation cell volume was optimized in the isobaric-isothermal ensemble using the Nose-Hover thermostat/barostat (5 ns simulation, coupling constants τ = 0.25 ps). Finally, production simulations were conducted in the isochoric-isothermal ensemble to generate 100 ns trajectories. The simulations were carried out using DL_POLY simulation engine [69-72], and the atomistic trajectories were analyzed using in-the-house developed analysis tools. The complementary simulations for the bulk water phase with varying density and NaCl solution with varying salt

concentrations have been carried out using the analogous simulation protocols. The NaCl solution was generated by randomly replacing water molecules with sodium and chloride ions and reoptimizing the cell volume if necessary.

2.5. Dielectric constant and density profiles

If a periodically oscillating electric field is applied to a solution containing molecular dipoles (e.g., water molecules), the dipoles will rotate to re-align with the field lines. The dipole orientation switches following the field oscillation with or without energy dissipation. In the case of a low field frequency, water molecules have time to orient themselves collectively without dissipating heat. In this regime, the collective dipole response is characterized by a static dielectric constant, ϵ_r. As the oscillation frequency increases to the microwave domain, more and more electric energy is converted into heat (Debye relaxation).

The static dielectric constant can be determined experimentally (e.g., dielectric/impedance spectroscopy) or theoretically using quantum or classical molecular modeling methods. Here, we calculated the dielectric response/susceptibility from the equilibrium fluctuations of total dipole moment fluctuations $\langle M^2 \rangle - \langle M \rangle^2$ via the following Clausius-Mosotti-type equation [66, 73]:

$$\epsilon_r = \lim_{\nu \to 0} \epsilon'(\nu) = 1 + \frac{\langle M^2 \rangle - \langle M \rangle^2}{3\epsilon_0 V k_B T} \quad (3)$$

where V is the volume of the aqueous phase and M is the total dipole moment of the ensemble of molecular dipoles ($\vec{M} = \sum_i \vec{\mu}_i$), k_B is the Boltzmann constant, T is the temperature. The frequency-dependent dielectric constant is calculated as the Laplace-Fourier transform of the time-derivative of the total dipole moment autocorrelation function [66, 73].

To calculate the dielectric constant as a function of the distance from the surface, referred to as the dielectric constant profile, we sliced the computational cell into bins parallel to the surface. Next, we calculated the collective dipole moment of water molecules in each bin. Finally, we applied eq. (3) to determine the local dielectric constant of that bin as a moving average:

$$\epsilon_r(z) = 1 + \frac{\langle M^2(z) \rangle - \langle M(z) \rangle^2}{3\epsilon_0 V(z) k_B T} \quad (5)$$

where z describes the position of the center of the slice in a direction normal to the surface. Notice that the number of molecular dipoles in each bin can vary along the simulation trajectory.

The water density profile is calculated as an average over all visited microstates (i.e., configurations, N_f) and represents the spatial distribution of water molecules in the z-direction [74-78]:

$$\rho(z) = \frac{1}{N_f} \sum_{i=1}^{N_f} \sum_{j=1}^{N} \delta\left(z - z_{ij}\right) \quad (6)$$

where the sums run over microstates (i) and water oxygen atoms (j) in the system and δ is the Dirac delta function.

3. Results and Discussion

3.1. Selection of water model to simulate dielectric properties

The dielectric relaxation spectroscopy of aqueous solutions probes the frequency-dependent response of molecules with permanent dipoles to the periodically oscillating electric field. In the case of aqueous solutions, each water molecule contributes a single dipole, but the dielectric response is a measure of the collective dynamics of the hydrogen-bonded network of water molecules [79]. A major feature of the water spectra is the Debye relaxation, which is characterized by a peak in the imaginary component and a sigmoid decrease of the real component of the dielectric response. At ambient conditions, these features appear around 19.24 GHz (8.27 ps) [79-81] (Fig. 4a,b).

It remains challenging to reproduce water dielectric spectra at varying temperatures and pressures using molecular dynamics simulations [79]. The polarizable and flexible interaction models showed promising results. However, three-body, rigid water models are preferred in many practical applications due to their compatibility with existing force fields for mineral/aqueous interfaces [82] or biomolecules [83-85]. In addition, the computational cost of explicit solvent simulations is significantly reduced if rigid, non-polarizable water models are used.

Unfortunately, few rigid water models can reproduce the static dielectric constant of liquid water at room temperature, and none can fully reproduce the dielectric spectra [79]. One of the exceptions is the OPC3 water model developed by Izadi and Onufriev [65]. The OPC3 gives an accurate estimate of the static dielectric constant of bulk water, but the dielectric spectrum is slightly shifted towards higher frequencies as compared with the experiment (Fig. 4a,b) [79].

The primary focus of this study is the static dielectric constant of the aqueous phase near the calcite/electrolyte interface, which is of paramount importance for SCMs' parametrization. The frequency-dependent response of the interfacial water and its Debye relaxation times are reported only for the water molecules in the first hydration layers – a space region corresponding to the inner Helmholtz layer.

3.2. Validation of the distance-dependent dielectric profiling

To model the dielectric constant profile in a direction normal to the surface, we implemented a slicing procedure similar to our previous studies of distance-dependent properties such as density, electric charge, or potential [74, 76-78, 86]. Before we applied the slicing protocol to the interfacial solution, we validated it for bulk liquid water at ambient conditions (Fig. 4c,d). First, the simulation cell was divided into bins along the z-direction (Fig. 4c). Next; we calculated the static dielectric constant for the whole cell and each isolated bin using eqs. 3,5. The values of the static dielectric constant are similar for the entire cell and each bin. However, the dipole ensembles are smaller for slices than for the whole cell, which results in subtle oscillations around the macroscopic value of 78 within each selected bin (Fig. 4d). These oscillations decrease with increasing bin size and increasing simulation time. To validate our slicing protocol, we used a 25 ns trajectory, which is sufficient to reproduce the bulk water properties [79] (Fig. 4). The dielectric constant profiles for the calcite/electrolyte interface were obtained from 100 ns simulation trajectories.

3.3. Water structure near the calcite (1014) surface

The calcite structure, as viewed along (1014) direction, consists of layers of alternating positive (Ca^{2+}) and negative (CO_3^{2-}) ions (Fig. 5a). These two types of ions interact differently with water molecules due to the opposite charges and charge distribution. Consequently, water molecules arrange differently around these ions. The first water solvation shell is split into two sublayers (two peaks, Fig. 5b). These sublayers are shifted by ~1 Å, which corresponds to the difference in the water-Ca^{2+} (first peak) and water-CO_3^{2-} (second peak) distances (Fig. 5c). The actual second hydration layer is located about 4.8-5 Å above the surface (Fig. 5b). There is a consensus in the literature that water molecules interacting with Ca^{2+} are found closer to the surface (~2.3 Å) than water molecules interacting with CO_3^{2-} ions (~3.3 Å), but the actual values of the peak position vary among reported studies [28, 53, 59, 87-89]. Our results are within the range of values reported previously (Fig. 5, Table 1). The interfacial water is affected strongly by the accumulation of electrolyte ions. Here we examine this phenomenon by carrying out molecular dynamics of the calcite/NaCl solution interface. First, we showed that the accumulation of electrolyte ions (Na^+, Cl^-) at the interface decreases water density in the first hydration layer. This is evident by comparing peak heights (Fig. 3b). Second, we observed that the first hydration layer and the second are split into two sublayers in the presence of an electrolyte. Finally, the hydration layers are positioned closer to the surface, suggesting that water molecules are pulled stronger than in the calcite/water interface case. The fact that the position of the hydration layers varies with the solution composition has already been reported in the simulation [59] and experimental [87] studies. However, the observation of subtle water-ordering propagation along with the water depletion and increased strength of the water-calcite interactions are novel.

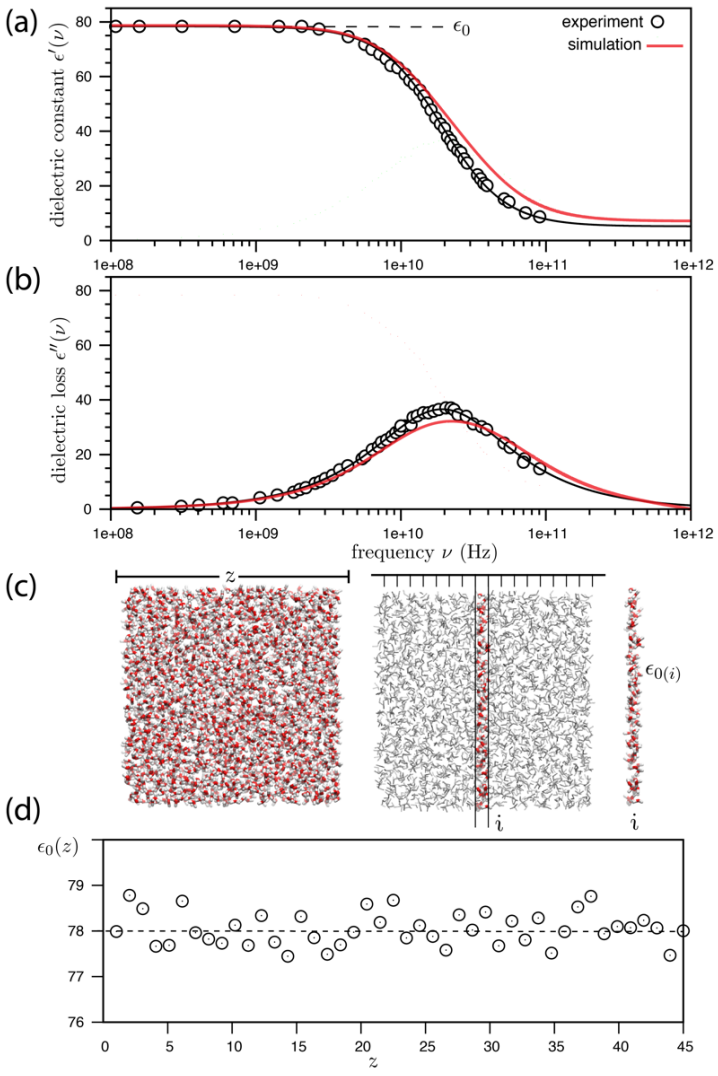

Figure 4. Accuracy of the OPC3 water model [90] in reproducing the dielectric spectra of bulk water at room temperature: real (a) and imaginary (b) parts of the dielectric response. The simulated spectrum was obtained from the Fourier transform of the time-dependent fluctuation of the total dipole moment [66] and compared to the experimental data taken from Kaatze [80, 81]. The slicing procedure implemented in this study to determine the distance-dependent dielectric properties and its validation are shown in the panels (c,d).

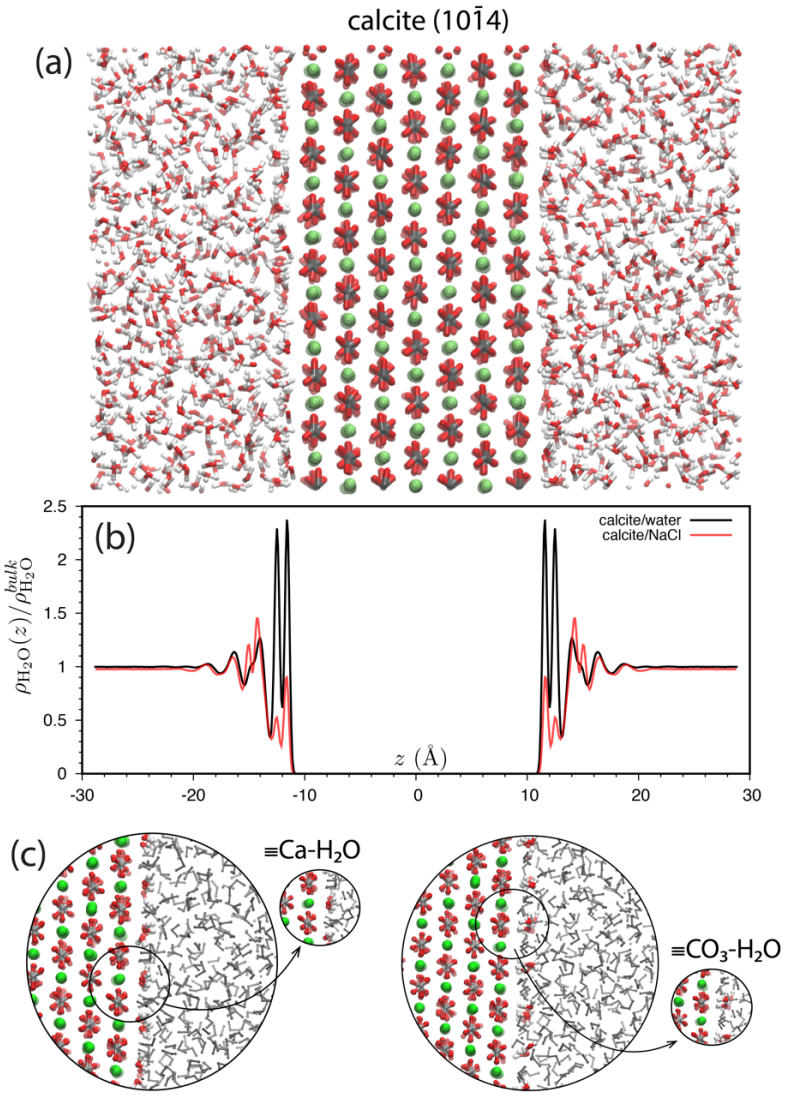

Figure 5. Calcite (10$\bar{1}$4) surface in contact with an aqueous solution (a) and corresponding water density profiles projected on normal to the surface (b). Two classes of water molecules in the first hydration layers: one interacts with the surface calcium ions and another with the surface carbonate ions (c). The water-calcite interactions are significantly weakened by the presence of electrolyte ions, as evident from the less structured oscillations. In the presence of electrolyte, the second hydration layer is also split into two peaks, similar to the first hydration layer.

3.4. Static dielectric profile of water at the calcite/electrolyte interface

By knowing how the dielectric constant of solution varies in space, we can improve the accuracy of many physicochemical models that rely on an implicit solvent representation (e.g., Born solvation, Marcus' electron transfer, Poisson-Boltzmann equation, self-consistent reaction field). These models reduce the computational complexity by replacing solvent molecules with a continuum polarizable medium. The continuum medium is characterized by a single dielectric constant value, even though medium polarizability should vary in space.

Unfortunately, our knowledge of dielectric constant variation in space is limited. The distance-dependent dielectric constant of interfacial solutions is not yet directly measurable. Few indirect measurements have been reported, but dielectric information was often extracted using a biasing assumption that confined or interfacial water has a lower dielectric constant than the bulk water [13, 17, 18]. In contrast, molecular modeling can directly probe the dielectric

properties of complex solutions. Surprisingly, most of the simulation studies suggest an increase in the dielectric constant of water near the hydrophobic and hydrophilic surfaces and oscillatory rather than monotonic distance-dependence [19-21].

Here, we carried out molecular dynamics simulations of the calcite/electrolyte interface to probe the distance-dependent dielectric constant of the interfacial solution. In Fig. 6, we show the profile of the static dielectric constant of aqueous solution across the simulation cell projected on a vector normal to the surface. The oscillations of dielectric constant near the calcite surface are similar to those reported previously for water and dipolar fluid near generic solid walls [19-21].

Note that our calcite slab is charge neutral, corresponding to the Point of Zero Charge conditions. The dielectric constant profile should vary for various charge states of the surface; however, to model these effects, one needs to use the reactive molecular dynamics simulations approaches that have been developed only for a few surfaces, see, for example, studies of the reactive goethite/electrolyte interfaces [75, 91, 92].

Table 1. Positions of the hydration layers at the calcite/electrolyte interface obtained in this study (in bold, Fig. 5) and reported previously [28] [53, 59, 87-89].

System	1st H_2O (Ca^{2+})	1st H_2O (CO_3^{2-})	2nd H_2O
Calcite/Water (this study)	**2.396**	**3.297**	**4.801**
Calcite/NaCl solution (this study)	**2.328**	**3.231**	**4.977**
Experiment	2.34 [88]	3.29 [88]	
	2.30 [89]	3.50 [89]	
	2.34 [28]	3.36 [28]	
	2.36 [87]	3.17 [87]	
Previous Simulations	2.2[b] [53]	3.2[b] [53]	5.0[b] [53]
	2.0[a] [59]	3.4[a] [59]	
	2.08[a] [87]	3.35[a] [87]	
	2.19[b] [87]	3.33[b] [87]	
	2.34[c] [87]	3.26[c] [87]	

[a]rigid-atom force field, [b]polarizable/flexible force field, [c]ab initio (Density Functional Theory)

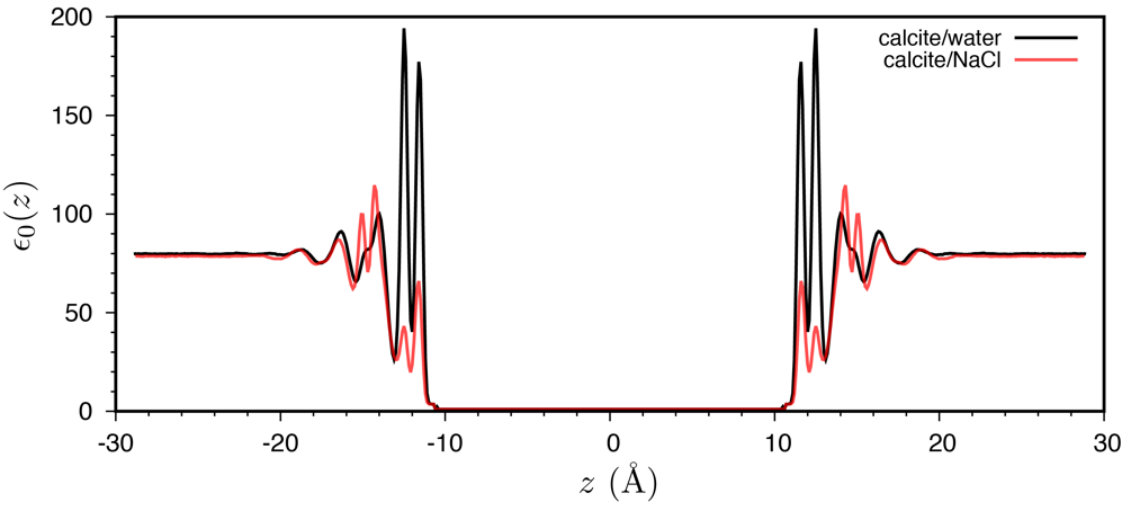

Figure 6. Distance-dependent dielectric profiles of solution in contact with the calcite ($\mathbf{10\bar{1}4}$) slab projected in a direction normal to the mineral surface. The positions of peaks on the dielectric profile are the same as the position of peaks on water density profiles (Fig. 3). In the absence of electrolyte ions, the surface hydration water that forms hydration shell around the surface exposed Ca^{2+} ions is less polarized (lower dielectric constant), than water associated with carbonate hydration shell (higher dielectric constant). The accumulation of electrolyte ions reduces the dielectric constant of the first hydration water layers, increases the dielectric constant of the second layer, and alters the positions of peaks due to the strong ordering of water around Na^+ ions accumulated near the carbonate ions.

3.5. Dielectric spectrum of the interfacial water

In Fig. 7, we compared the frequency-dependent dielectric constant and dielectric loss within the first hydration layer with those of the bulk water. The water in the first hydration layer has a slower response time to the oscillating electric field as measured by the Debye relaxation time (τ_D) and Debye relaxation frequency (ν_D). The Debye relaxation of water molecules at the calcite interface is about four and two times slower than the bulk water phase in the case of the calcite/water and calcite/NaCl solution interfaces, respectively. The electrolyte ions disrupt the hydrogen bonding network of the interfacial water resulting in almost twice faster Debye relaxation of interfacial water molecules in the presence of electrolyte ions as compared with the calcite/water interface.

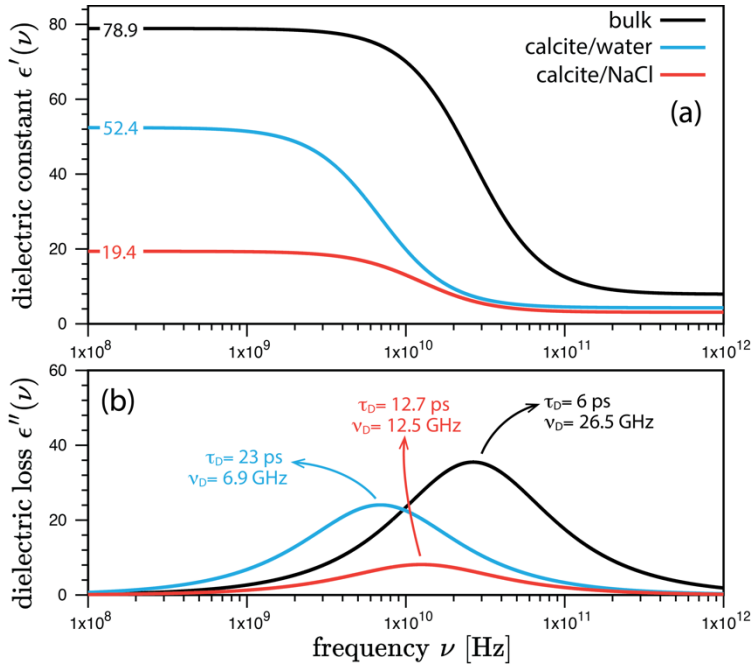

Figure 7. Frequency-dependent dielectric response of the interfacial water: a) real component (dielectric constant, ε'(ν)) and b) imaginary component (dielectric loss, ε''(ν)). The Debye relaxation time (τ_D) and Debye relaxation frequency (ν_D) characterize the peak position on dielectric loss curves.

3.6. Water density and dielectric constant are linearly correlated

The dielectric constant and water density profiles resemble each other in terms of peak positions, oscitation amplitudes, and oscillation phases (compare Figs. 5b, 6). This resemblance has been observed before; see, for example, reports by Bonthuis et al. [19, 20, 93].

The correlation between the dielectric constant and water density is not surprising. First, the polarization vector ***P*** that governs the dielectric response is defined as a dipole moment density, and because each water molecule contributes a single dipole vector, the fluid density and ***P*** have to be correlated. Second, the linear correlation between the dielectric constant and density is suggested by the Clausius-Mosotti-type relationships (see eq. 3). For example, if the total dipole moment fluctuations are neglected, then the dielectric constant is determined by the dipole density ($\rho = N/V$) and dipole moment (μ) of a single water molecule [94]:

$$\epsilon_r \approx 1 + \frac{1}{3\epsilon_0 k_B T}\frac{N\mu^2}{V} = 1 + \frac{1}{3\epsilon_0 k_B T}\rho\mu^2 \quad (7)$$

Although the above formula neglects the dipole-dipole interactions and it is valid only for the isotropic gas-like phase [94], it emphasizes an intimate connection between the dielectric constant and the dipole density.

Here, we report that density-dielectric constant correlation is, to a large extent, preserved also in a complex system with a phase boundary and a non-uniform electrolyte ions distribution at the interface. By analyzing the relationship between the local density and the local dielectric constant, we found that the distance-dependent dielectric constant can be approximated by the normalized water density as follows:

$$\epsilon_r(z) = \frac{\rho(z)}{\rho(bulk)}\epsilon_r(bulk) \quad (8)$$

where $\epsilon_r(bulk)$ is the relative dielectric constant of water phase that is far from the surface, and $\rho(z)$, $\rho(bulk)$ are distance-dependent and bulk water density, respectively.

In Fig. 8, we compare the dielectric profile calculated explicitly via eq. (5) and approximated from the density profile using eq. (8). The calculated and approximated values of the dielectric constant trace each other almost perfectly (Fig. 8). There are only a few subtle discrepancies in the peak heights (see insert Fig. 8).

In general, intimate relationships between density profiles and properties are expected. The modern statistical mechanical models of the charged solid/electrolyte interfaces that are based either on the classical Density Functional Theory (c-DFT) [95] or the Ornstein-Zernike integral equation [95-97] describe the system using density profiles or pair correlation functions, respectively. In particular, cDFT expresses the grand thermodynamic potential and free energy as functionals of density profiles for all components in the solution.

3.7. Computational shortcut for estimation of dielectric constant profiles

The dielectric responses calculated from the atomistic trajectory converge very slowly, and their accurate estimation requires computationally expensive simulation runs, for example, exceeding 50-100 ns in complex and nonuniform systems [79]. In contrast, the water density profile converges within a few nanoseconds. The correlation between the dielectric constant and water density profiles offers a computational shortcut for calculating the interfacial water polarizability and its distance dependence from a shorter simulation trajectory. By exploiting this relationship, one can get instant insight into distance-dependent dielectric properties and incorporate this linear relationship in the physicochemical models relying on the implicit solvent representation.

3.8. Dielectric decrement and excluded volume effects

As shown in Fig. 6, the dielectric constant of water near the calcite surface is significantly lower in the presence of electrolyte ions. This is not surprising; a decrease of the dielectric constant with increasing electrolyte concentration, referred to as the dielectric decrement, is expected and has been reported [98-101]. The dielectric decrement is mostly due to the dielectric saturation effect, which can be defined as a loss of water molecule rotation freedom in a strong electric field present in the ion vicinity. An additional contribution is due to the long-range disruptive or constructive effect of ions on the water hydrogen bond network - a phenomenon behind ion classification into kosmotropes (order-makers) and chaotropes (disorder-makers) and arrangement into Hofmeister-type affinity series [102].

The layering of water near the surface is due to the strong hydration of the calcite surface, and it is affected by the accumulated electrolyte ions (Fig. 5b). We carried out two additional simulations to understand if the dielectric constant oscillation near the calcite surface is due to the water density oscillations or due to the dielectric decrement caused by electrolyte ions. Specifically, we carried out the molecular dynamics simulations of *i)* NaCl solution at room temperature with varying NaCl concentration and *ii)* pure liquid water at ambient conditions with artificially varying water density.

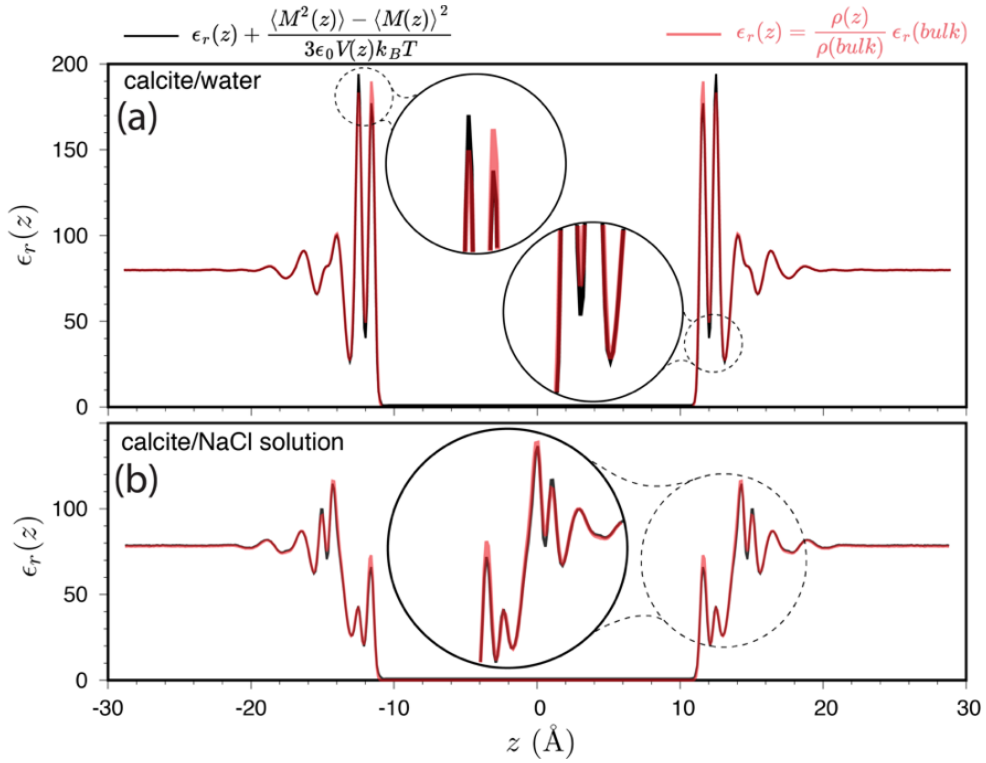

Figure 8. Correlation between dielectric constant profile calculated from the fluctuations of the total dipole moment, eq. (5), and estimated from the water density profile via eq. (8) for the calcite $(10\bar{1}4)$/water (a) and calcite $(10\bar{1}4)$/electrolyte solution (b) interfaces.

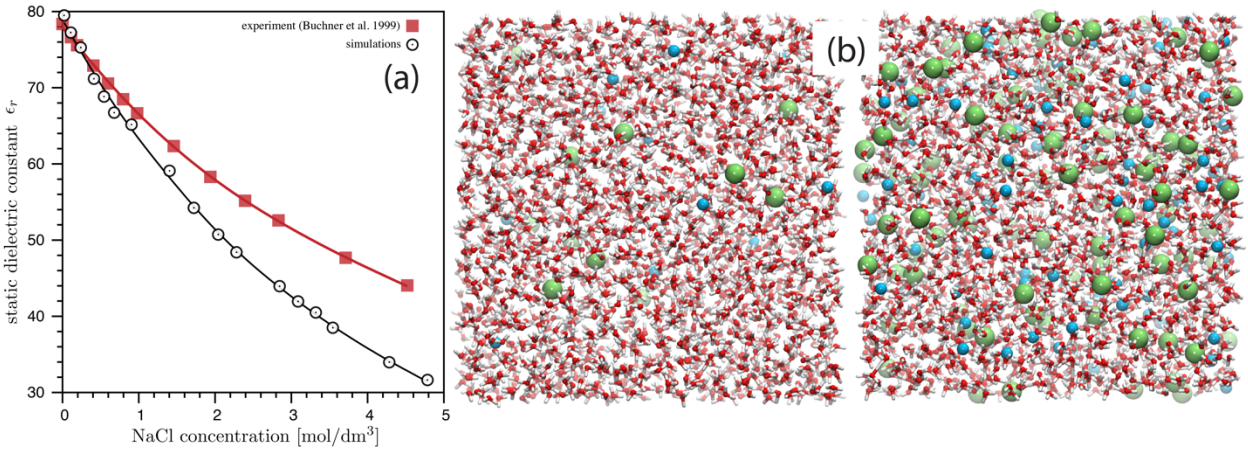

Figure 9. Comparison of the molecular dynamics simulations and experimental data of the variation in the solution dielectric constant with the NaCl concentration (a). The snapshots of the simulation cells of diluted and concentrated NaCl solution (b): cyan sphere represent Na^+ ions, and the green sphere represents Cl^- ions. The experimental data are taken from Buchner et al. [103].

In the first setup, we carry out molecular dynamics simulations of NaCl solutions (Fig. 9). The dielectric decrement, that is, a decrease in dielectric constant with an increasing salt concentration, is initially linear and can be approximated as:

$$\varepsilon_r(c) = \varepsilon_r(0) + b \cdot c \quad (9)$$

where $\varepsilon_r(0)$ stands for the static dielectric constant of pure water (i.e., c = 0), and b is the decrement coefficient given in dm^3/mol. The coefficient b is negative and describes how sensitive the dielectric constant and the hydrogen-bond network are to the presence of ions. At higher electrolyte concertation, the dielectric decrement becomes non-linear due to the overlapping of ion hydration shells. However, here we focus on the linear regime, which is more important for comparing electrolyte ion vs density depletion effect on dielectric constant at the mineral/electrolyte interface. The more robust molecular/physicochemical modeling of dielectric decrement can be found elsewhere [104, 105].

Our main goal in modeling the dielectric decrement in NaCl solutions is to compare the dielectric constant–concentration dependence in the bulk solution and near the calcite surface. The dielectric decrement for the first layers near the calcite surface that resides between the surface and the β-plane is more rapid than in the isolated bulk electrolyte solution. The estimated value of b coefficient is about twice larger for the electrolyte near the mineral surface (b = -33.04 dm^3/mol) than in the bulk solution (b =-14.8 dm^3/mol). Note that we predict a slightly faster dielectric decrement in the bulk solution, b =-14.8 dm^3/mol, than observed experimentally, b =-11.9 dm^3/mol (Fig. 9). We concluded that interfacial water density fluctuations seem to be responsible for a more rapid decrease of dielectric constant with increasing electrolyte concentration than observed in the bulk electrolyte solutions.

The effect of charge distribution at the interface on the dielectric constant is difficult to model in isolation; however, by simulating the density effect on the bulk water dielectric constant in the absence of ions and charged surface, we can get an insight into the role of density fluctuations. Fig. 10 shows how decreasing water density at ambient conditions reduces the dielectric constant. Here, we fixed the temperature and pressure but artificially changed the simulation cell volume to alter the effective water density in the cell.

The water molecules prefer to remain in a tetrahedral arrangement, and therefore by increasing the volume of the simulation cell, we created cavities in the liquid water. As a result, the decrease in the dielectric constant is a consequence of the formation of water/vapor interfaces, but on the macroscopic scale, it is equivalent to lower effective density. Here, we again model dielectric decrement caused by varying density as a linear function of effective water density:

$$\varepsilon_r(\rho) = a + b\,\rho \quad (10)$$

where b is a decrement coefficient given in cm^3/g, and a is the static dielectric constant of water in a hypothetical state of an infinite dilution. This simulation aimed to compare the strength of the density-dielectric constant relationship for water near the calcite surface and water in the bulk phase. Here, we focus only on the slope of eq. (10). Notice that eq. (8) is equivalent to eq. (10) if a = 0 and then $b = \epsilon_r(bulk)/\rho^{\mathrm{bulk}}$. The coefficient b is always positive and describes how rapidly the dielectric constant increases with the increasing water density ρ. The linear relationship is not expected to hold at low density due to cavity formations and at high density due to ice-like cluster formation.

We obtain b=78.7 g/cm3 by fitting a few data points in the vicinity of 1 g/cm3 density maker if a is set to 0. A similar value (b = 78.9) is obtained for the slope of the density-dielectric constant relationship at the calcite/electrolyte interface. The identical strength of the density-dielectric constant relationship in both simulations suggests that knowledge of the water density is sufficient to determine the dielectric constant at ambient conditions.

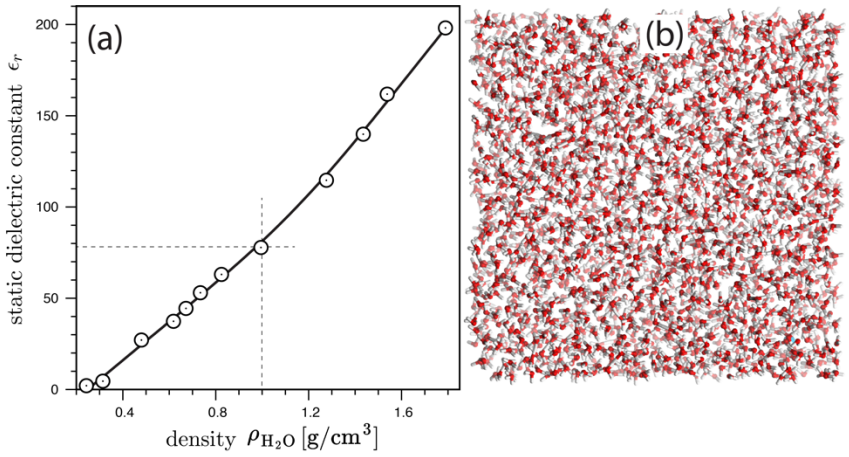

Figure 10. Molecular dynamics simulations of the water dielectric constant as a function of effective water density at ambient conditions (a). The water/vapor interfaces spontaneously form if the effective density is much lower than ~1 g/cm^3. In panel (b) we showed an example of the simulation cell for ρ equals 1.3 g/cm^3. The water density was adjusted by varying the size of the primary simulation cell while the number of water molecules remained fixed.

3.9. Capacitances

SCMs of the calcite/electrolyte interface consist of several adjustable parameters, whose values are determined by fitting experimental data such as potentiometric or electrokinetic titrations [27, 28, 31-33]. Among many SCMs parameters, the capacitances are one of the most challenging to determine in a physiochemically consistent fashion [27, 28, 31-33, 106].

Here, we used eq. (1) to estimate the capacitance values. The position of hydration layers and the average dielectric constant for the solution between these layers are obtained by analyzing density and dielectric constant profiles (Table 2). The capacitance values are between 0.47 and 1.2 F/m^2 and correspond to dielectric constant between 19 and 78. These values agree well with those reported by Heberling et al. [27, 88]. For example, if the Stern layer thickness is equal to 3.5 Å, then the capacitance values able to fit experimental data are between 0.1 F/m^2 (dielectric constant ε=6) and 2.8 F/m^2 (for ε=78.5) [27]. The recommended value of c_1 equals 0.45 F/m^2, and it corresponds to the effective dielectric constant equals 18 (thickness 3.5 Å) [27] or 12 (thickness 4.6 Å) [28]. Recently, a new version of TLM was proposed with slightly different water-surface distances and revised capacitances c_1=0.2 F/m^2 and c_2=1.5 F/m^2, which correspond to dielectric constants of ice-like ε=6 and bulk-like ε=74.5 water phases, respectively [88].

Our molecular dynamics simulations suggest a thicker Stern layer than indicated by previous studies (compare Tables 1 and 2). This is because we consider not only the most probable position of the water molecules, a peak on the density plot, but a full range of water positions in the first hydration layer at the calcite/electrolyte interface. In the case of the sodium chloride solution, we estimated the value of the dielectric constant as equal to 19.38 and the capacitance of the Stern layer as equal to 0.46 (Table 2); both values are in agreement with those reported by Heberling et al. [27].

It is important, to emphasize that simulation results are sensitive to the choice of interaction parameters. For example, the position of the hydration layers varies between reported simulation studies (see Table 1). Here, the most important is the ability of the water model to correctly describe the polarization within the hydration layers. The agreement between the capacitances reported here, and those reported by Heberling et al. [27] is sensitive to the force-field parameter values; however, it is expected to hold if only the water model can accurately represent the dielectric properties.

The changes in the fluid properties confined between the β- and d-planes (c_2, ε_2) are very small despite the noticeable variation in the d-plane position. In contrast, the variation of the fluid properties between the calcite surface and β-plane as a function of electrolyte concertation is large, despite a very tiny dependence on the β-plane position. In the presence of NaCl, we obtained c_1 value that is close to the one used originally by Heberling et al. [27].

Due to the linear relationship between capacitances and dielectric constant of the solution contained between parallel-plate capacitors, one can propose a simple linear relationship between capacitance and NaCl concentration

that reflects the dielectric constant decrease with increasing salt content. We performed molecular dynamics simulations in two extreme cases of infinitely diluted NaCl solution (calcite/water interface) and concentrated NaCl solution (1M). These simulations provided two endpoints for linear interpolating distances and capacitances as a function of NaCl electrolytes (Table S2, see Supporting Information). To illustrate the effect of capacitance on the SCM model predictions, we calculated how the diffuse layer potential as a function of pH varies with varying electrolyte concentration in models with concentration-dependent capacitance with constant capacitance (Fig. S1, Supporting Information). Suppose the capacitance varies linearly with the electrolyte concentration. In that case, the electrokinetic potential is lower than in the case of the fixed capacitance value due to more considerable surface potential screening by the charges accumulated in the rigid part of EDL (larger capacitances, see Supporting Information).

One of the interesting observations reported in Table 2 is that the values of two TLM's capacitances (c_1, c_2) are very similar in the calcite/water interface case and significantly different for the calcite/NaCl electrolyte solution.

Table 2. The average dielectric permittivity and capacity of the inner and outer-Helmholtz planes of the EDL calculate ed using the eq. (1).

System	d_1 (Å)	ε_1	c_1 (F/m^2)	d_2 (Å)	ε_2	c_2 (F/m^2)
Calcite/water	3.899	52.42	1.190	6.592	78.66	1.057
Calcite/NaCl solution (1M)	3.701	19.38	0.464	7.279	78.43	0.954

Concluding, here we showed that by using molecular dynamics simulation, we could model the distance-dependent dielectric properties of aqueous solution in contact with the mineral surfaces. Moreover, by applying compartmentalization consistent with the electric double-layer model employed by SCMs, one can estimate the larger-scale model parameter values (here, capacitances). We illustrated this approach for the calcite $(10\bar{1}4)$/electrolyte interface. We showed that capacitances should vary with the electrolyte composition/concentration to account for variations in water dipole ordering caused by changes in the surface charge and ion accumulation near the interface.

4. Conclusions

We developed the computational protocol to calculate the distance-dependent dielectric constant profile for the aqueous solutions in contact with mineral surfaces. Our protocol was validated for the bulk water solution and then applied to the calcite $10\bar{1}4$ crystal surface/aqueous solution interface.

The dielectric constant profile shows an oscillatory behavior that is linearly correlated to the water density profile, confirming the previous observations of the resemblance between the dielectric constant and fluid density for fluids near the hydrophilic and hydrophobic surfaces [19, 20, 93]. Dielectric properties converge slowly, and their accurate estimation requires computationally expensive simulation runs of 50-100 ns in the case of complex or nonuniform systems [79]. In contrast, the water density profile converges rapidly within a few nanoseconds. The correlation between the dielectric constant profile and the water density profile offers a computational shortcut for inferring interfacial water polarizability and its distance dependence without the requirement of running long simulations.

We used tailored simulations to examine if interfacial water was in the dielectric saturation state or in an ice-like state. The interfacial water resembles the rigid ice-like structure in dense regions, with the amplitude of the dielectric constant exceeding the bulk water value and much slower relaxation times, confirming an ice-like frozen state. However, the presence of the electrolyte ions disrupts ice-like ordering, primarily by depleting the interfacial water density, and secondary by rearranging water dipoles within ion hydration shells. Our results suggest that water density fluctuation governs the dielectric properties near the surface. The dielectric increment, a drop in the dielectric constant due to the presence of the electrolyte ions, can also be explained based on the changes in the water density alone.

Macroscopic theoretical models based on the continuum solvent description assume that the dielectric constant decreases monotonically with decreasing distance to the surface. In contrast, molecular simulations, including those presented here, show that the solvent polarizability oscillates near the surface. We showed that molecular and mesoscale pictures agree with each other if we spatially average the dielectric constant obtained from molecular dynamics simulations over the distances relevant to the mean-field representation, e.g., plane separation in SCMs.

We also showed that values of capacitances used in SCM could be estimated using molecular simulations insight into the spatially averaged dielectric constants and positions of hydration layers. The most significant limitation of existing SCMs is a lack of the physiochemically constrained capacitances [27, 28], often leading to unrealistic values of the corresponding dielectric constant [27, 28, 31-33, 106]. Here, we showed how SCM capacitances could be inferred from the molecular dynamics simulations in the case of the calcite ($10\bar{1}4$)/aqueous solution interface.

The implications of our study are much broader than SCMs parametrization because the dielectric constant of a solution is of vital importance in all theoretical models that treat solvent as a continuum (solvation [107], charge transfer [108], activity coefficients [109], the Lifshitz theory of van der Waals forces [110]). The accuracy of these models will improve significantly if we include the distance-dependent dielectric constant of the intervening medium at micro- and mesoscale levels.

Our results also have implications for our understanding of the hydration forces - oscillatory interactions observed experimentally if two sufficiently smooth surfaces approach each other at distances comparable with a few molecular diameters of water [110]. First, oscillations in the dielectric constants translate to the oscillations in the Hamaker constant according to the Lifshitz theory of van der Waals forces [110]. Second, oscillations in water density translate to the oscillation in the elastic modules with surface separation, leading to additional mechanical components of a physicochemical origin.

Acknowledgments

This work was supported by the U.S. Department of Energy (DOE) Chemical Sciences, Geosciences, and Biosciences Division under Contract DE-AC02-05CH11231.

References

[1] J.A. Davis, R.O. James, J.O. Leckie, Surface Ionization and Complexation at Oxide-Water Interface .1. Computation of Electrical Double-Layer Properties in Simple Electrolytes, J Colloid Interf Sci 63(3) (1978) 480-499.
[2] D.A. Dzombak, F.M.M. Morel, Surface Complexation Modeling: Hydrous Ferric Oxide, Wiley, New York, 1990.
[3] J. Lutzenkirchen, Surface Complexation Modelling, Elsevier, Amsterdam, 2006.
[4] J. Lyklema, Fundamentals of Interface and Colloid Science, Academic Press, London, 1991.
[5] G.E. Brown, V.E. Henrich, W.H. Casey, D.L. Clark, C. Eggleston, A. Felmy, D.W. Goodman, M. Gratzel, G. Maciel, M.I. McCarthy, K.H. Nealson, D.A. Sverjensky, M.F. Toney, J.M. Zachara, Metal oxide surfaces and their interactions with aqueous solutions and microbial organisms, Chem Rev 99(1) (1999) 77-174.
[6] J. Lutzenkirchen, Comparison of 1-pK and 2-pK versions of surface complexation theory by the goodness of fit in describing surface charge data of (hydr)oxides, Environ Sci Technol 32(20) (1998) 3149-3154.
[7] W. Piasecki, Determination of the parameters for the 1-pK triple-layer model of ion adsorption onto oxides from known parameter values for the 2-pK TLM, J Colloid Interf Sci 302(2) (2006) 389-395.
[8] K.F. Hayes, G. Redden, W. Ela, J.O. Leckie, Surface Complexation Models - an Evaluation of Model Parameter-Estimation Using Fiteql and Oxide Mineral Titration Data, J Colloid Interf Sci 142(2) (1991) 448-469.
[9] J.O.M. Bockris, S.U.M. Khan, Surface Electrochemistry. A Molecular Level Approach, Springer1993.

[10] T.J. Webb, The free energy of hydration of ions and the electrostriction of the solvent, J Am Chem Soc 48 (1926) 2589-2603.
[11] J.O.M. Bockris, A.K.N. Reddy, M. Gamboa-Aldeco, Modern Electrochemistry, Fundamentals of Electrodics, Kluwer, New York, 2000.
[12] B.E. Conway, J.O. Bockris, I.A. Ammar, The Dielectric Constant of the Solution in the Diffuse and Helmholtz Double Layers at a Charged Interface in Aqueous Solution, T Faraday Soc 47(7) (1951) 756-766.
[13] E. Mccafferty, V. Pravdic, A.C. Zettlemoyer, Dielectric Behaviour of Adsorbed Water Films on Alpha-Fe2o3 Surface, T Faraday Soc 66(571) (1970) 1720-+.
[14] H.B. Cui, K. Takahashi, Y. Kano, H. Kobayashi, Z.M. Wang, A. Kobayashi, Dielectric properties of porous molecular crystals that contain polar molecules, Angew Chem Int Edit 44(40) (2005) 6508-6512.
[15] A.R. Haidar, A.K. Jonscher, The Dielectric-Properties of Zeolites in Variable Temperature and Humidity, J Chem Soc Farad T 1 82 (1986) 3535-3551.
[16] T. Ishida, T. Makino, C.J. Wang, Dielectric-relaxation spectroscopy of kaolinite, montmorillonite, allophane, and imogolite under moist conditions, Clay Clay Miner 48(1) (2000) 75-84.
[17] O. Teschke, E.F. de Souza, Dielectric exchange: The key repulsive or attractive transient forces between atomic force microscope tips and charged surfaces, Appl Phys Lett 74(12) (1999) 1755-1757.
[18] L. Fumagalli, A. Esfandiar, R. Fabregas, S. Hu, P. Ares, A. Janardanan, Q. Yang, B. Radha, T. Taniguchi, K. Watanabe, G. Gomila, K.S. Novoselov, A.K. Geim, Anomalously low dielectric constant of confined water, Science 360(6395) (2018) 1339-+.
[19] D.J. Bonthuis, S. Gekle, R.R. Netz, Dielectric Profile of Interfacial Water and its Effect on Double-Layer Capacitance, Phys Rev Lett 107(16) (2011) 166102.
[20] D.J. Bonthuis, S. Gekle, R.R. Netz, Profile of the Static Permittivity Tensor of Water at Interfaces: Consequences for Capacitance, Hydration Interaction and Ion Adsorption, Langmuir 28(20) (2012) 7679-7694.
[21] V. Ballenegger, J.P. Hansen, Dielectric permittivity profiles of confined polar fluids, J Chem Phys 122(11) (2005) 114711.
[22] D. Croize, F. Renard, J.P. Gratier, Compaction and Porosity Reduction in Carbonates: A Review of Observations, Theory, and Experiments, Adv Geophys 54 (2013) 181-238.
[23] J.W. Morse, F.T. Mackenzie, Geochemistry of Sedimentary Carbonates, Elsevier, Amsterdam, 1990.
[24] J.J. Predali, J.M. Cases, Zeta Potential of Magnesian Carbonates in Inorganic Electrolytes, J Colloid Interf Sci 45(3) (1973) 449-458.
[25] L. Madsen, Calcite: Surface Charge, in: P. Somasundaran (Ed.) Encyclopedia of Surface and Colloid Science, CRC Press, Boca Raton, 2015, pp. 801-813.
[26] I. Sondi, J. Biscan, N. Vdovic, S.D. Skapin, The electrokinetic properties of carbonates in aqueous media revisited, Colloid Surface A 342(1-3) (2009) 84-91.
[27] F. Heberling, T.P. Trainor, J. Lutzenkirchen, P. Eng, M.A. Denecke, D. Bosbach, Structure and Reactivity of the Calcite-Water Interface, J Colloid Interf Sci 354(2) (2011) 843-857.
[28] F. Heberling, D. Bosbach, J.D. Eckhardt, U. Fischer, J. Glowacky, M. Haist, U. Kramar, S. Loos, H.S. Muller, T. Neumann, C. Pust, T. Schafer, J. Stelling, M. Ukrainczyk, V. Vinograd, M. Vucak, B. Winkler, Reactivity of the Calcite-Water-Interface, From Molecular Scale Processes to Geochemical Engineering, Appl Geochem 45 (2014) 158-190.

[29] S.L. Stipp, M.F. Hochella, Structure and Bonding Environments at the Calcite Surface as Observed with X-Ray Photoelectron-Spectroscopy (XPS) and Low-Energy Electron-Diffraction (LEED), Geochim Cosmochim Ac 55(6) (1991) 1723-1736.
[30] M. Wolthers, L. Charlet, P. Van Cappellen, The Surface Chemistry of Divalent Metal Carbonate Minerals; a Critical Assessment of Surface Charge and Potential Data Using the Charge Distribution Multi-Site Ion Complexation Model, Am J Sci 308(8) (2008) 905-941.
[31] P. Van Cappellen, L. Charlet, W. Stumm, P. Wersin, A Surface Complexation Model of the Carbonate Mineral-Aqueous Solution Interface, Geochim Cosmochim Ac 57(15) (1993) 3505-3518.
[32] O.S. Pokrovsky, J. Schott, Surface chemistry and dissolution kinetics of divalent metal carbonates, Environ Sci Technol 36(3) (2002) 426-432.
[33] F. Heberling, T. Klacic, P. Eng, T. Preocanin, J. Lützenkirchen, Structure and Surface Complexation of the Calcite-Water-Interface, Goldschmidt 2019, Barcelona, Spain, 2019.
[34] M. Prus, K. Szymanek, J. Mills, L.N. Lammers, W. Piasecki, K. Kedra-Krolik, P. Zarzycki, Electrophoretic and potentiometric signatures of multistage CaCO3 nucleation, J Colloid Interf Sci 544 (2019) 249-256.
[35] M. Prus, C.H. Li, K. Kedra-Krolik, W. Piasecki, K. Lament, T. Begovic, P. Zarzycki, Unseeded, spontaneous nucleation of spherulitic magnesium calcite, J Colloid Interf Sci 593 (2021) 359-369.
[36] Q.R.S. Miller, E.S. Ilton, O. Qafoku, D.A. Dixon, M. Vasiliu, C.J. Thompson, H.T. Schaef, K.M. Rosso, J.S. Loring, Water Structure Controls Carbonic Acid Formation in Adsorbed Water Films, J Phys Chem Lett 9(17) (2018) 4988-4994.
[37] A. Anderson, W.R. Ashurst, Interfacial Water Structure on a Highly Hydroxylated Silica Film, Langmuir 25(19) (2009) 11549-11554.
[38] D.B. Asay, S.H. Kim, Evolution of the adsorbed water layer structure on silicon oxide at room temperature, J Phys Chem B 109(35) (2005) 16760-16763.
[39] S.L.S. Stipp, Toward a conceptual model of the calcite surface: Hydration, hydrolysis, and surface potential, Geochim Cosmochim Ac 63(19-20) (1999) 3121-3131.
[40] C.J.R. Braithwaite, Carbonate Sediments and Rocks, Whittles, Dunbeath, 2005.
[41] A. Pavese, M. Catti, S.C. Parker, A. Wall, Modelling of the thermal dependence of structural and elastic properties of calcite, CaCO3, Phys Chem Miner 23(2) (1996) 89-93.
[42] A. Pavese, M. Catti, G.D. Price, R.A. Jackson, Interatomic Potentials for Caco3 Polymorphs (Calcite and Aragonite), Fitted to Elastic and Vibrational Data, Phys Chem Miner 19(2) (1992) 80-87.
[43] N.H. de Leeuw, S.C. Parker, Modeling absorption and segregation of magnesium and cadmium ions to calcite surfaces: Introducing MgCO3 and CdCO3 potential models, The Journal of Chemical Physics 112(9) (2000) 4326-4333.
[44] N.H. deLeeuw, S.C. Parker, Atomistic simulation of the effect of molecular adsorption of water on the surface structure and energies of calcite surfaces, J Chem Soc Faraday T 93(3) (1997) 467-475.
[45] N.H. de Leeuw, S.C. Parker, Surface structure and morphology of calcium carbonate polymorphs calcite, aragonite, and vaterite: An atomistic approach, J Phys Chem B 102(16) (1998) 2914-2922.
[46] N.H. de Leeuw, S.C. Parker, K.H. Rao, Modeling the competitive adsorption of water and methanoic acid on calcite and fluorite surfaces, Langmuir 14(20) (1998) 5900-5906.

[47] N.H. de Leeuw, S.C. Parker, J.H. Harding, Molecular dynamics simulation of crystal dissolution from calcite steps, Phys Rev B 60(19) (1999) 13792-13799.
[48] D.K. Fisler, J.D. Gale, R.T. Cygan, A shell model for the simulation of rhombohedral carbonate minerals and their point defects, Am Mineral 85(1) (2000) 217-224.
[49] S. Kerisit, S.C. Parker, J.H. Harding, Atomistic simulation of the dissociative adsorption of water on calcite surfaces, J Phys Chem B 107(31) (2003) 7676-7682.
[50] T.D. Archer, S.E.A. Birse, M.T. Dove, S.A.T. Redfern, J.D. Gale, R.T. Cygan, An interatomic potential model for carbonates allowing for polarization effects, Phys Chem Miner 30(7) (2003) 416-424.
[51] R. Kristensen, S.L.S. Stipp, K. Refson, Modeling steps and kinks on the surface of calcite, J Chem Phys 121(17) (2004) 8511-8523.
[52] O.W. Duckworth, R.T. Cygan, S.T. Martin, Linear free energy relationships between dissolution rates and molecular modeling energies of rhombohedral carbonates, Langmuir 20(7) (2004) 2938-2946.
[53] S. Kerisit, S.C. Parker, Free energy of adsorption of water and metal ions on the {1014} calcite surface, J Am Chem Soc 126(32) (2004) 10152-10161.
[54] D. Spagnoli, S. Kerisit, S.C. Parker, Atomistic simulation of the free energies of dissolution of ions from flat and stepped calcite surfaces, J Cryst Growth 294(1) (2006) 103-110.
[55] J.D. Gale, P. Raiteri, A.C.T. van Duin, A reactive force field for aqueous-calcium carbonate systems, Phys Chem Chem Phys 13(37) (2011) 16666-16679.
[56] P. Fenter, S. Kerisit, P. Raiteri, J.D. Gale, Is the Calcite-Water Interface Understood? Direct Comparisons of Molecular Dynamics Simulations with Specular X-ray Reflectivity Data, J Phys Chem C 117(10) (2013) 5028-5042.
[57] P. Raiteri, R. Demichelis, J.D. Gale, Thermodynamically Consistent Force Field for Molecular Dynamics Simulations of Alkaline-Earth Carbonates and Their Aqueous Speciation, J Phys Chem C 119(43) (2015) 24447-24458.
[58] P. Raiteri, A. Schuitemaker, J.D. Gale, Ion Pairing and Multiple Ion Binding in Calcium Carbonate Solutions Based on a Polarizable AMOEBA Force Field and Ab Initio Molecular Dynamics, J Phys Chem B 124(17) (2020) 3568-3582.
[59] P. Raiteri, J.D. Gale, D. Quigley, P.M. Rodger, Derivation of an Accurate Force-Field for Simulating the Growth of Calcium Carbonate from Aqueous Solution: A New Model for the Calcite-Water Interface, J Phys Chem C 114(13) (2010) 5997-6010.
[60] C.L. Freeman, J.H. Harding, D.J. Cooke, J.A. Elliott, J.S. Lardge, D.M. Duffy, New forcefields for modeling biomineralization processes, J Phys Chem C 111(32) (2007) 11943-11951.
[61] S. Hwang, M. Blanco, W.A. Goddard, Atomistic Simulations of Corrosion Inhibitors Adsorbed on Calcite Surfaces I. Force field Parameters for Calcite, The Journal of Physical Chemistry B 105(44) (2001) 10746-10752.
[62] A.L. Rohl, K. Wright, J.D. Gale, Evidence from surface phonons for the (2 × 1) reconstruction of the (10$\bar{1}$4) surface of calcite from computer simulation, Am Mineral 88(5-6) (2003) 921-925.
[63] R.A. Jackson, G.D. Price, A Transferable Interatomic Potential for Calcium Carbonate, Molecular Simulation 9(2) (1992) 175-177.
[64] M.T. Dove, B. Winkler, M. Leslie, M.J. Harris, E.K.H. Salje, A new interatomic potential model for calcite: Applications to lattice dynamics studies, phase transition, and isotope fractionation, Am Mineral 77(3-4) (1992) 244-250.

[65] S. Izadi, A.V. Onufriev, Accuracy limit of rigid 3-point water models, J Chem Phys 145(7) (2016) 074501.
[66] P. Zarzycki, B. Gilbert, Temperature-dependence of the dielectric relaxation of water using non-polarizable water models, Phys Chem Chem Phys 22 (2020) 1011-1018
[67] A. Sengupta, Z. Li, L.F. Song, P.F. Li, K.M. Merz, Parameterization of Monovalent Ions for the OPC3, OPC, TIP3P-FB, and TIP4P-FB Water Models (vol 61, pg 869, 2021), J Chem Inf Model 61(7) (2021) 3734-3735.
[68] A. Sengupta, Z. Li, L.F. Song, P.F. Li, K.M. Merz, Parameterization of Monovalent Ions for the OPC3, OPC, TIP3P-FB, and TIP4P-FB Water Models, J Chem Inf Model 61(2) (2021) 869-880.
[69] W. Smith, T.R. Forester, Parallel Macromolecular Simulations and the Replicated Data Strategy .2. The Rd-Shake Algorithm, Comput Phys Commun 79(1) (1994) 63-77.
[70] W. Smith, T.R. Forester, Parallel Macromolecular Simulations and the Replicated Data Strategy .1. The Computation of Atomic Forces, Comput Phys Commun 79(1) (1994) 52-62.
[71] I.T. Todorov, W. Smith, K. Trachenko, M.T. Dove, DL_POLY_3: new dimensions in molecular dynamics simulations via massive parallelism, J Mater Chem 16(20) (2006) 1911-1918.
[72] M.F. Guest, A.M. Elena, A.B.G. Chalk, DL_POLY - A performance overview analysing, understanding and exploiting available HPC technology, Molecular Simulation 47(2-3) (2021) 194-227.
[73] D. van der Spoel, P.J. van Maaren, H.J.C. Berendsen, A systematic study of water models for molecular simulation: Derivation of water models optimized for use with a reaction field, J Chem Phys 108(24) (1998) 10220-10230.
[74] P. Zarzycki, C.A. Colla, B. Gilbert, K.M. Rosso, Lateral water structure connects metal oxide nanoparticle faces, J Mater Res 34(3) (2019) 456-464.
[75] P. Zarzycki, K.M. Rosso, Surface Charge Effects on Fe(II) Sorption and Oxidation at (110) Goethite Surfaces, J Phys Chem C 122(18) (2018) 10059-10066.
[76] P. Zarzycki, B. Gilbert, Long-Range Interactions Restrict Water Transport in Pyrophyllite Interlayers, Sci Rep-Uk 6 (2016) 25278.
[77] P. Zarzycki, K.M. Rosso, Molecular Dynamics Simulation of the AgCl/Electrolyte Interfacial Capacity, J Phys Chem C 114(21) (2010) 10019-10026.
[78] P. Zarzycki, S. Kerisit, K.M. Rosso, Molecular Dynamics Study of the Electrical Double Layer at Silver Chloride Electrolyte Interfaces, J Phys Chem C 114(19) (2010) 8905-8916.
[79] P. Zarzycki, B. Gilbert, Temperature-dependence of the dielectric relaxation of water using non-polarizable water models, Phys Chem Chem Phys 22(3) (2020) 1011-1018.
[80] U. Kaatze, Complex Permittivity of Water as a Function of Frequency and Temperature, J Chem Eng Data 34(4) (1989) 371-374.
[81] U. Kaatze, Reference liquids for the calibration of dielectric sensors and measurement instruments, Meas Sci Technol 18(4) (2007) 967-976.
[82] R.T. Cygan, J.J. Liang, A.G. Kalinichev, Molecular models of hydroxide, oxyhydroxide, and clay phases and the development of a general force field, J Phys Chem B 108(4) (2004) 1255-1266.
[83] W.D. Cornell, P. Cieplak, C.I. Bayly, I.R. Gould, K.M. Merz, D.M. Ferguson, D.C. Spellmeyer, T. Fox, J.W. Caldwell, P.A. Kollman, A second generation force field for the simulation of proteins, nucleic acids, and organic molecules (vol 117, pg 5179, 1995), J Am Chem Soc 118(9) (1996) 2309-2309.

[84] B.R. Brooks, R.E. Bruccoleri, B.D. Olafson, D.J. States, S. Swaminathan, M. Karplus, Charmm - a Program for Macromolecular Energy, Minimization, and Dynamics Calculations, J Comput Chem 4(2) (1983) 187-217.
[85] W.R.P. Scott, P.H. Hunenberger, I.G. Tironi, A.E. Mark, S.R. Billeter, J. Fennen, A.E. Torda, T. Huber, P. Kruger, W.F. van Gunsteren, The GROMOS biomolecular simulation program package, J Phys Chem A 103(19) (1999) 3596-3607.
[86] P. Zarzycki, Interfacial Water Screens the Protein-Induced Transmembrane Voltage, J Phys Chem B 119(4) (2015) 1474-1482.
[87] S.J.T. Brugman, P. Raiteri, P. Accordini, F. Megens, J.D. Gale, E. Vlieg, Calcite (104) Surface-Electrolyte Structure: A 3D Comparison of Surface X-ray Diffraction and Simulations, J Phys Chem C 124(34) (2020) 18564-18575.
[88] F. Heberling, T. Klačić, P. Raiteri, J.D. Gale, P.J. Eng, J.E. Stubbs, T. Gil-Díaz, T. Begović, J. Lützenkirchen, Structure and Surface Complexation at the Calcite(104)–Water Interface, Environ Sci Technol 55(18) (2021) 12403-12413.
[89] P. Geissbuhler, P. Fenter, E. DiMasi, G. Srajer, L.B. Sorensen, N.C. Sturchio, Three-dimensional structure of the calcite-water interface by surface X-ray scattering, Surf Sci 573(2) (2004) 191-203.
[90] S. Izadi, R. Anandakrishnan, A.V. Onufriev, Building Water Models: A Different Approach, J Phys Chem Lett 5(21) (2014) 3863-3871.
[91] P. Zarzycki, D.M. Smith, K.M. Rosso, Proton Dynamics on Goethite Nanoparticles and Coupling to Electron Transport, Journal of Chemical Theory and Computation 11(4) (2015) 1715-1724.
[92] P. Zarzycki, K.M. Rosso, Energetics and the Role of Defects in Fe(II)-Catalyzed Goethite Recrystallization from Molecular Simulations, ACS Earth and Space Chemistry 3(2) (2019) 262-272.
[93] D.J. Bonthuis, R.R. Netz, Beyond the Continuum: How Molecular Solvent Structure Affects Electrostatics and Hydrodynamics at Solid–Electrolyte Interfaces, The Journal of Physical Chemistry B 117(39) (2013) 11397-11413.
[94] F. Kremer, A. Schönhals, Broadband Dielectric Spectroscopy, Springer, Berlin, 2003.
[95] D.N. Petsev, F. van Swol, L.J.D. Frink, Molecular Theory of Electric Double Layers, IOP Publishing, 2021.
[96] L. Blum, D. Henderson, Statistical mechanics of electrolytes at interfaces, in: D. Henderson (Ed.), Fundamentals of Inhomogeneous Fluids, CRC Press, Boca Raton, 1992, pp. 239–276.
[97] P. Attard, Electrolytes and the Electric Double Layer, Advances in Chemical Physics1996, pp. 1-159.
[98] J. Barthel, R. Buchner, M. Munsterer, Electrolyte Data Collection: Part 2: Dielectric Properties of Water and Aqueous Electrolyte Solutions, Dechema, Frankfurt, 1995.
[99] J. Barthel, R. Buchner, Dielectric permittivity and relaxation of electrolyte solutions and their solvents, Chemical Society Reviews 21(4) (1992) 263-270.
[100] R.A. Robinson, R.H. Stokes, Electrolyte Solutions, Butterworth & Co., London, 1970.
[101] Y. Marcus, Ions in solution and their solvation, Wiley, Hoboken, 2015.
[102] Y. Marcus, Effect of Ions on the Structure of Water: Structure Making and Breaking, Chem Rev 109(3) (2009) 1346-1370.
[103] R. Buchner, G.T. Hefter, P.M. May, Dielectric relaxation of aqueous NaCl solutions, J Phys Chem A 103(1) (1999) 1-9.

[104] H. Gao, Y. Chang, C. Xiao, An analytical expression for dielectric decrement law, AIP Advances 10(4) (2020) 045109.
[105] S. Seal, K. Doblhoff-Dier, J. Meyer, Dielectric Decrement for Aqueous NaCl Solutions: Effect of Ionic Charge Scaling in Nonpolarizable Water Force Fields, The Journal of Physical Chemistry B 123(46) (2019) 9912-9921.
[106] M. Takeya, A. Ubaidah, M. Shimokawara, H. Okano, T. Nawa, Y. Elakneswaran, Crude oil/brine/rock interface in low salinity waterflooding: Experiments, triple-layer surface complexation model, and DLVO theory, J Petrol Sci Eng 188 (2020).
[107] B. Mennucci, R. Cammi, Continuum Solvation Models in Chemical Physics: From Theory to Applications, Wiley, West Sussex, 2007.
[108] V. May, O. Kühn, Charge and Energy Transfer
Dynamics in Molecular Systems, Wiley, Weinheim, 2011.
[109] K.S. Pitzer, Activity coefficients in electrolyte solutions, Boca Raton, CRC Press.
[110] J.N. Israelachvili, Intermolecular and Surface Forces, 2 ed., Academic Press, Amsterdam, 1992.